The Redshift Distribution of Gamma-Ray Burst and its Implication to the Universe

Desalegn Abebaw Maru

A Thesis Submitted to the Department of Applied Physics

School of Applied Natural Science

Presented in Partial Fulfillment of the Requirement for the Degree of Master’s in physics (Astrophysics)

Office of Graduate Studies

Adama Science and Technology University

November, 2022

Adama, Ethiopia

The Redshift Distribution of Gamma-Ray Burst and Its Implication to the Universe

Desalegn Abebaw Maru

Adivisor: Anno Kare (Ph.D)

A Thesis Submitted to the department of Applied Physics,

School of Applied Natural Science

Presented in Partial Fulfillment of the Requirement for the Degree of Master's in physics (Astrophysics)

Office of the Graduate Studies

Adama Science And Technology University

November, 2022

Adama, Ethiopia

Declaration

I declare that this thesis entitled "**The Redshift Distribution of Gamma-Ray Burst and Its Implication to the Universe**" is my own work. That is, it has not been submitted to any University for similar purpose. The references used in this thesises are duly recognized by proper citations.

________________ ____________________ ________________________

Name of Student Signiture Date

Recommendation

We, the advisors of this thesis, hereby certify that we have read the revised version of the thesis entitled "**The Redshift Distribution of Gamma-Ray Burst and Its Implication to The Universe**" prepared under our guidance by Desalegn Abebaw Maru submitted in partial fulfillment of the requirements for the degree of Master's of Science in physics (Astrophysics). Therefore, we recommend that the submission of revised version of the thesis to the department following the applicable procedures.

Major Advisor	Signiture	Date

Approval Page

We, the advisors of the thesis entitled "**The Redshift Distribution of Gamma-Ray Burst and Its Implication to The Universe**" and developed by Desalegn Abebaw Maru, hereby certify that the recommendation and suggestion made by the board of examiners are appropriately incorporated into the final version of the thesis.

Major Advisor	Signiture	Date

We, the undersigned, members of the Board of Examiners of the thesis by Desalegn Abebaw Maru, have read and evaluated the thesis entitled "**The Redshift Distribution of Gamma-Ray Burst and Its Implication to The Universe**" and examined the candidate during the open defense. This is, therefore, to certify that the thesis is accepted for partial fulfilment for the requirement of the degree of Master of Science in physics (Astrophysics).

Chairperson	Signature	Date
Internal Examiner	Signature	Date
External Examiner	Signature	Date

Final approval and acceptance of the thesis is contingent upon submission of its final copy to the Office of Postgraduate Studies (OPGS) through the Department Graduate Council (DGC) and School Graduate Committee (SGC).

Department Head	Signature	Date

School Dean	Signature	Date
Office of Postgraduate Studies, Dean	Signature	Date

ACKNOWLEDGMENT

First of all, I would like to give great thanks to God who gave me the chance to live and complete this work. Next, I express my appreciation to my advisor Dr. Anno Kare who has given me a lot of helpful suggestion, advice and comments for completion of this thesis. Finally, I would like thank my intimate friend Mohamed Ahmed who helped me in many situations and circumstances.

Table of Contents

List of Tables

List of Figures

List of Acronyms and Abbreviations

BAT/Burst Alert Telescope

CGRO/Compton Gamma Ray Observatory

Dec/Declination

EGRET/Energetic Gamma-Ray Experiment Telescope

GLAST/Gamma-Ray Large Area Space Telescope

GeV/Giga electron Volt

GRB/Gamma-Ray Burst

HETE/High Energy Transient Explorer

SNe Ia /supernovae type Ia

INTEGRAL/International Gamma-Ray Astrophysics Laboratory

ISM/interstellar medium

K-S/Kolmogorov- Smirnov

LGRB/Long Gamma ray Burst

z/Redshift

RA/Right Ascentoin

SGRB/Short Gamma ray Burst

SED/ Spectral Energy Distribution

SFR/Star Formation Rate

TeV/Terra electron Volt

BATSE/Burst and Transient Source Experiment

UVOT/Ultra Violate and Optical Telescope

XRT/X-Ray Telescope

Abstract

Gamma-ray bursts (GRBs) are the most energetic explosions found ever in the universe and produce huge amounts of energy in gamma-rays over a short time period ranging from a few milliseconds to thousands of seconds. The peak luminosity, peak fluence and the redshift distribution of recent long gamma-ray bursts (GRBs) were predicted through the Monte Carlo simulations. The GRB LF and redshift distribution are constructed in the frameworks of different evolution models using the maximum likelihood method. GRB were related to the rate of formation of stars. This analysis contained some parameters such as the peak energy distribution of bright swift bursts. Integrations and derivatives were done by the ExceLab 365. In this work we have seen that the luminosity function is distributed mostly around 4.8E+51 ergs/sec. *The SFR of long GRB were in to three groups:1. The SFR increased up to some point of z and became decrease after some points z, 2. the SFR increased up to some point and became constant after some point, and the last the SFR increased constantly in any given value of z. We have calculated the comoving rate of gamma ray burst and the star formation rate of GRB by relating it to the long GRB explosion of supernova type II. And also, we have evaluated the observed peak fluence, flux and luminosity distance of the long GRB.*

Keyword: Gamma-Ray Burst, Redshift, Monte Carlo, cosmology, supernovae.

1 Introduction

1.1 Background of The Study

Even though gamma-ray bursts in astrophysics have been studied intensively for years, it has failed to provide a comprehensive understanding of these phenomena. There is little knowledge of the property of uniform bursts due to the heterogeneous nature of their bursts, which makes classification difficult(Gehrels et al. 2008). In any case, Gamma Ray Bursts (GRBs) were found in the late 1960s by military satellites observing the Earth for mystery atomic weapons tests. In spite of the fact that cosmologists proceeded to collect information over 30 years, and small advance was made in understanding these occasions due to their exceptionally temporal nature. It was not indeed clear whether these objects were portion of the neighborhood or far off Universe. The primary real breakthrough came within the early 1990s with the dispatch of the Compton Gamma Beam Observatory. In specific, the Burst and Transitory Source Experiment (BATSE) gotten positions for a few thousand GRBs to show that they were distributed uniformly over the complete sky. This was the primary suggestive prove that GRBs were cosmological substance.

The problem then was that although BATSE could detect GRBs, it couldn't position them accurately enough on the sky to allow for follow-up observations. In 1997 finally, obtained conclusive proof that GRBs occupy the distant reaches of the Universe. An absorption spectrum was detected in the optical transient spectrum of the GRB970508 GRB. When a star is examined through a telescope, a continuous spectrum will show interruptions where particular wavelengths of energy have been absorbed by the atoms of the gas cloud, re-emitted in an arbitrary direction, and scattered away from our telescope beam. This is referred to as an absorption spectrum, and it can be found at a cosmic redshift along the line of sight. This implied that the GRB itself was located at cosmic distance, which was considerably further away(McBreen, Foley, and Hanlon 2009).

Since the late 1990s, it has practically become normal procedure to identify optical transients and the GRB afterglows. High Energy Transient Explorer (HETE), SWIFT, and International Gamma-Ray Astrophysics Laboratory (INTEGRAL) are just a few examples of current satellites whose main missions include quickly detecting and triangulating GRB positions and relaying this information to other satellites and ground-based observatories via the Gamma Ray Burst Coordinates Network for follow-up observations at other wavelengths. With the help of this network, it is now possible to monitor a GRB at various wavelengths within one minute of the burst's initial satellite detection. The nature of these potent explosions must be uncovered quickly because GRBs are transitory, fleeting events Gamma-ray bursts (GRBs) have long been suggested as a complementary probe to type Ia supernovae (SNe Ia) and to investigate the cosmic microwave background's expansion history in the high-redshift cosmos, primarily because they are luminous enough to be observed at wider distances.

Gamma-ray bursts (GRBs) are the most intense electromagnetic sources in the Universe and can be described as the most energetic explosions at cosmological distances after years of extensive research. Their prompt gamma-ray radiation, lasting between a fraction of a second to the several thousand seconds, corresponds to an energy release of $10^{51}\ to\ 10^{54}$ joule. A big star collapsing or two dense objects merging together are the two most plausible cataclysmic events that could have produced it(C. Wang, Peng, and Huang 2022). A burst of γ-rays is what is known as a gamma-ray burst (GRB). The term gamma-ray refers to the energy range from tens of keV to several MeV, based on the typical bandpass of spaceborne GRB detectors (e.g., Burst and Transient Source Experiment (BATSE) onboard the Compton Gamma-Ray Observatory (CGRO), Burst Alert Telescope (BAT) onboard The Neil Gehrels Swift Observatory, and Gamma-ray Burst Observatory, GBM onboard the Fermi Gamma-Ray Space Telescope). The GRB prompt emission is the common name for this burst emission in the hard-X-ray/ γ soft-ray band(Yi-zhong Fan and Piran 2018).

Gamma-ray bursts are strong flashes of high energy that travel from cosmological distances to Earth, where they can be easily detected. GRBs can therefore be employed to explore the far reaches of the Universe regardless of their physical origin(Rossi and Mochkovitch 2006). Also, it is known that gamma rays are bright (approximately a few photons $cm^{-2}\ s^{-1}$flux in the 50–300 keV band) flashes that are observable at Earth approximately once per day. The Compton Gamma Ray Observatory's BATSE instrument revealed that they are dispersed over the sky and exhibit very feeble bursts. (Paciesas et al. 1999). The actual source of this emission remains a mystery fifty years after its discovery and despite the use of numerous specialized space-based equipment. Only 17 GRBs have recorded redshifts after four years into the age of gamma-ray burst (GRB) afterglow investigations (Claussen et al. 2013).

Figure 1.1: A typical Gamma-Ray Burst from explosion of supernovae(Valle 2016)

Moreover, CGRO, Swift and Fermi are three missions that provide us great information about phenomena of GRB. Table 1.1 shows the telescopes on board of these satellites with their energy ranges.

Table 1.1: Different types of GRB detector instruments (SD Barthelmy, TL Cline, P Butterworth 2000)

Mission	Telescope	Energy Range
CGRO	BATSE	20kev-1000kev
	OSSE	50kev-10Mev
	COMPTEL	1Mev-10Mev
	EGRET	20Mev-30Gev
swift	BAT	15Kev-150Kev
	XRT	0.2kev-10kev
	UVOT	170nm-600nm
FERMI	LAT	20Mev-300Gev
	GBM	8kev-30Mev

Currently, two missions are still in progress: Swift and Fermi. Swift was given its name after a bird that hunts insects. Swift, a little spacecraft that scans the sky in search of GRBs. These Rapid instruments detect optical and x-ray radiation. On the other hand, the Fermi Gamma-Ray Large Area Space Telescope (GLAST) is intended to detect objects at or above the upper end of the Swift range by continuously scanning the whole sky.

A lot of work was put towards determining the total prompt energy release (peak luminosity) in GRBs before the first redshift determination of GRBs. This was done by analyzing the brightness distribution of GRB occurrences. Fluence and flux are factors that can be measured while measuring gamma ray bursts, and their measurement is dependent on the detector's bandpass sensitivity range(Ryde 2011).

The first GRB peculiarity is their enormous observed fluence, between 10^{-7} and 10^{-5} erg cm^{-2}. The major event, the prompt high-energy emission, is typically seen in the gamma-rays and lasts for a few to tens of seconds. It is then typically followed by its opposite, a persistent multi-wavelength emission known as the afterglow phase. Following the occurrence of the prompt emission, the multi-wavelength afterglow emission starts. Typically, only a small portion of the total energy of the GRB is released during this period. After the prompt emission, the X-ray afterglow phase often begins hundreds of seconds to many hours later. The detector's sensitivity range (bandpass) determines how much fluence or flux may be measured for a certain GRB. The recent afterglow discoveries have illustrated that multiwavelength studies are the key to our further understanding of GRBs. Swift is designed specifically to study GRBs and their afterglow multiple wavelengths.

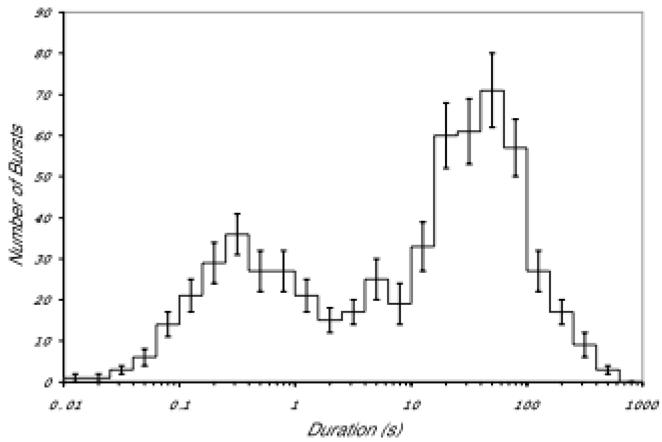

Figure 1.2: Burst duration vs. number of GRBs detected by BATSE

One important hypothesis is that the power-law decrease of the source flux is caused by a transition in the spectrum from the gamma-ray to optical band. It can take up to 1000 seconds for this break to cross into the optical band from the X-ray band, hence it is crucial to make observations in these bands within the first 1000 seconds. Although it currently appears that all lengthy GRBs have X-ray afterglows, not all of them have intense optical or radio afterglows (at least after several hours). While optical extinction may be to blame, it's also plausible that in some instances the optical (and X-ray) afterglow exists but decays far more quickly. To answer many issues, prompt, high-quality X-ray, UV, and optical measurements during the first few minutes to hours of the afterglow are essential. Since flares can develop in the decaying emission, constant observation is crucial. The information of afterglow mechanism and sites will be well-understood because Swift's capacity to identify X-ray spectral lines and edges. This information includes density, ionization, elemental abundance, and outflow characteristics(Jones, Stark, and Ellis 2018). Swift will enable the observation of lines during the early bright phase of the afterglow, during which they are best detected. Star-forming regions are embedded in large columns of neutral gas and dust. BATSE uses three trigger intervals Δt = 64, 256 and 1024 ms. The bias introduced by this process, occurs because bursts could have true durations T larger or shorter than Δt(Dermer, C. D. 2002).

The simultaneous detection of high X-ray absorption, coupled with photometric measurements with Swift, will determine whether dust and gas are present. Continuous monitoring over the first few hours to days will indicate whether dust is building up (as a result of condensation out of an expanding hot wind) or disappearing as a result of ablation and evaporation.

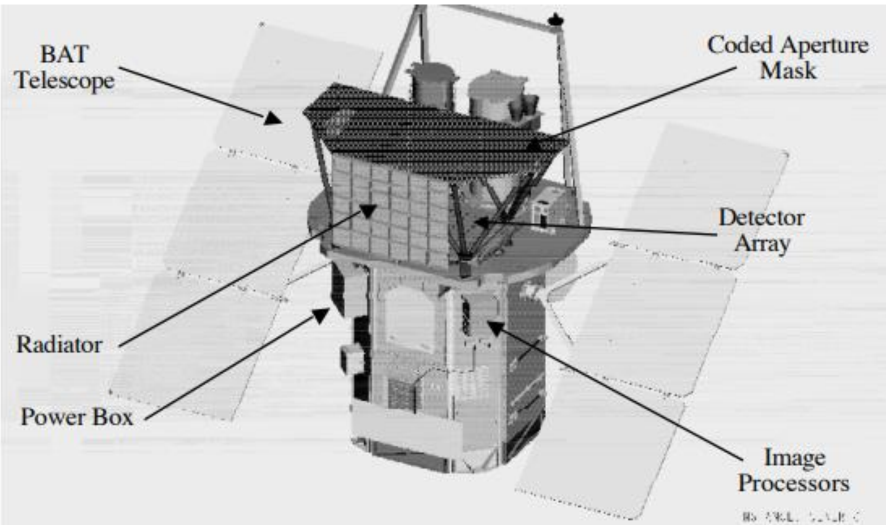

Figure 1.3: The Swift spacecraft showing the BAT (the D-shaped coded-aperture mask), the X-Ray Telescope (XRT and Ultra Violate Telescope UVOT instruments (the two tubes in the back), and the solar panels. BAT is composed of the Detector Array, the Coded Mask, the thermal Radiator, the 2 Image Processors, and the Power Control box.

To reveal the Detector Array and the Struts that support the Mask, the Graded-Z Fringe Shield side walls have been taken down. Some properties of Gamma- Ray Burst

- GRBs have a high luminosity, making them visible at high redshifts.
- When they propagate towards us, gamma-ray photons do not experience extinction. However, the interstellar medium will cause the optical photons from supernovae to become extinct.
- Stellar mass objects are thought to be the origin of GRBs. Therefore, since their host galaxy has a low mass at high redshifts, the intrinsic luminosity of GRBs shouldn't be dependent on it.
- Long GRBs triggered by the death of massive stars, which have been shown to be associated with supernovae(Stanek et al. 2003), provide a complementary technique for measuring star formation rate. They also represent a unique probe of the initial mass function and the star formation of massive stars at very high redshifts. GRBs offer the exciting opportunity to detect the Population.

GRBs can be used in conjunction with other instruments to measure dark energy and cosmic expansion. For the purposes of the Hubble diagram, type Ia supernovae (SNe Ia) are now regarded as ideal standard candles. In 1998, two teams' studying distant SNe Ia discovered independent evidence that the expansion of the Universe is speeding up(Perlmutter and Berkeley), which is attributed to the mysterious component-dark energy. The observation of brightness distances of high redshift SNe Ia is connected to the direct evidence for the universe's current acceleration. The expansion history of our universe, or the redshift distance relation, is the greatest approach to measure the characteristics of dark energy. The ideal way to investigate the characteristics of dark energy is to measure it over a broad redshift range, however, SNe Ia can only be found at low redshifts at $z = 2.0$.

In many areas of astrophysics, the high-redshift ($z > 6$) star formation history (SFH) is significant. The low component of the galaxy luminosity function makes it difficult for current technologies to estimate the direct star formation rate (SFR). A supplemental method for assessing the SFR is provided by long GRBs that are caused by the death of big stars (Wanderman and Piran 2010). Massive stars have brief lifetimes, therefore the SFR can be thought of as their death rate.

1.2 Statement of The Problem

We are living in dynamic Universe subjected to change and motion of objects contained in it. However, the redshift distribution of the universe is not determined precisely in recent years of data collected by detector instruments. The detection of high redshift galaxy can better constrain the star formation rate. Then we are interested in to predict the distribution of GRB's redshift in the Universe.

1.3 Significance of The Study

Gamma-Ray Bursts are produced by spectacular events in the Universe such as stars exploding, matter falling into black holes and celestial objects colliding. By collecting gamma rays, we are able to see these violent events and can judge exactly how they shape the Universe. By using redshift data, we can reveal how an object in space (star/planet/galaxy) is moving compared to us. It lets us to measure a distance for the most distant (and therefore oldest) objects in our Universe.

By estimating the redshift distribution of the gamma ray burst, the gamma-ray burst related parameters such as luminosity function, star formation rate, flux and fluence etc can be studied for further analysis.

1.4 Objectives

1.4.1 General Objective

The general objective of the study is:
To determine the redshift distribution of the universe and to study their effect to the Universe.

1.4.2 Specific Objectives

The specific objectives of our study are:

- ✓ To find the GRB comoving rate and luminosity function
- ✓ To predict the impact of uncertainty in the predicted gamma ray burst rate
- ✓ To drive the expected distribution of observed redshift, peak flux and peak fluence of swift satellite.

2 Literature Review

Gamma-ray bursts (GRBs) are the most powerful explosions known in the universe. Sensitive measurements of the high-energy spectra of GRBs can place important constraints on the burst environments and radiation processes.

Gamma-ray bursts (GRBs) are the most luminous explosion in the Universe (Zhang & M´esz´aros 2004). They offer exciting possibilities for studying astrophysics in extreme conditions, e.g., radiative processes in highly relativistic ejecta (Huang, Dai, and Lu 2000;Yi-zhong Fan and Piran 2018). The overall GRB's observed fluences range from 10^{-4} ergs/$cm^2$to 10^{-7}ergs/cm^2 the lower limit depends, of course, on the characteristics of the detector and not on the bursts themselves. This corresponds to isotropic luminosity of 10^{51}–10^{52} ergs/sec, making GRB's the most luminous objects in the sky. However, we know today that most GRB's are narrowly beamed and the corresponding energies are only 10^{51} $ergs$(Metzger et al. 1997) making them comparable to supernovae in total energy release.

Seven GRBs with photon energies ranging from 100 MeV to 18 GeV were detected by the High Energy Gamma-ray Experiment Telescope (EGRET, the High Energy Gamma-ray Detector on the Compton Gamma-ray Observatory) (Dingus et al. 2009). In some cases, this very high energy emission was delayed for more than an hour after the burst (Ackermann et al. 2013). The boundary between the two recognized burst classes is often drawn in a two-dimensional plot of spectral intensity versus duration, where short bursts appear to be slightly stronger than long bursts(Ackermann et al. 2013; Connaughton et al. 2015).

Based on a class of theoretical models currently in vogue, the observed burst and the resulting afterglow radiation are synchrotron emissions of a non-thermal electrons accelerated by strong shocks in the relativistic flow (Piran 2000). In this model, the high energy emission from the burst itself is emitted by internal shocks created by collisions between regions at different velocities (Lorentz factor) in the relativistic outflow, while the low afterglow energy (radio, optical and X-rays) is believed to be released by an external shock, where the effluent enters the surrounding medium. The discovery of the afterglows of gamma-ray bursts (Frontera, L Amati, E Costa, JM Muller 2000) allowed to pinpoint their position in the X-ray and optical bands. This opened a new era focused at measuring the spectroscopic redshifts of these sources. This is not surprising since the total fluence of short GRBs is also much lower than the long bursts, and since afterglow brightness broadly scales with fluence the faintness consistent with expectations.

Over 100 brief GRBs have now been found by Swift, of which 70% have been identified by X-ray afterglow. About 25% of observations that try to pinpoint optical afterglow do so successfully. The distances to practically all short GRBs are estimated from these galaxies, which are commonly identified in these data as possible host galaxies.

2.1 Spectral Properties of Gamm-Ray Burst

2.1.1 How to Describe Spectrum

Spectra from GRBs are not thermal. On the other hand, a non-thermal spectrum reaches significantly higher energies and often exhibits a power-law flux distribution. This calls for the acceleration of the electrons in a non-equilibrium setting (e.g., shocks, magnetic reconnection sites) (Tsvi Piran and Ehud Nakar 2010). Photons must be gathered at specific time intervals in order to obtain a spectrum. In order to analyze the evolution of spectral features, spectra should ideally be recovered over a short period of time because GRBs are extremely changeable events. The spectrum is typically shown in high-energy astronomy as intensity vs frequency (or energy), not wavelength (which is more commonly used in optical astronomy). There are four ways to display the same spectrum:

I. Raw photon count spectrum C(E), expressed in $s^{-1}KeV^{-1}$. This shows the number of detected photons as a function of energy bin. Even though the intrinsic spectrum is regular, the count spectrum is strongly influenced by the detector's instrumental response function since detectors often have varied sensitivities in different energy bins (e.g., power law or thermal).

II. The "photon number" spectrum N(E), in photons $cm^{-2}s^{-1}KeV^{-1}$, has been extracted after experimental response function effects have been eliminated, simulating the real specific photon flux detected from Earth. The quantity N(E)dE indicates how many photons are contained in the energy bin dE. The photon number spectrum is the easiest to get since photons are measured individually in X-ray and γ-ray astronomy.

III. The specific flux density spectrum (usually expressed as F_{ν} in units of erg $cm^{-2}s^{-1}\cdot Hz^{-1}$, or EN(E) in units of erg$cm^{-2}s^{-1}KeV^{-1}$. When individual photons cannot be directly counted, a spectrum like this is typically utilized in IR, optical, and UV astronomy. Alternatively, the measurement and display of the photon energy per unit frequency (or unit energy) is used. $F_\nu d\nu$ or EN(E)dE is the photon energy in the frequency bin dν or energy bin dE as a result.

IV. The energy spectrum (ν$F_\nu$or E^2N(E), usually expressed as νF_ν or E^2N(E) (e.g., in units of erg·cm^{-2} s^{-1}), is a spectrum of electromagnetic waves. A spectral energy distribution (SED) is another name for this. One can quickly determine how the source's bolometric energy is dispersed in frequency or energy by viewing such a spectrum(Du et al. 2022).

For GRB, N(E)dE spectra are usually constructed first. Several spectral models have been applied to fit such spectra.

2.2 Progenitors of Gamma-Ray Burst

It is difficult to identify the source of the systems causing gamma-ray bursts because are so far from Earth. The association of some long gamma-ray bursts with supernovae and the fact that their host galaxies rapidly form stars provide very strong evidence that long gamma-ray bursts are associated with massive stars. The most widely accepted mechanism for the origin of long-lived GRBs is the collapse model (MacFadyen and Woosley 1999), in which the core of an extremely massive, low-metallic, rapidly rotating star collapses into a black hole in its final stages of evolution. Material near the star's core rains down toward the center and swirls around in a dense accretion disk. The in fall of this material into a black hole drives a pair of relativistic jets out along the rotational axis, which pummel through the stellar envelope and eventually break through the stellar surface and radiate as gamma rays. Some alternative models replace the black hole with a newly formed magnetar, although most other aspects of the model (the collapse of the core of a massive star and the formation of relativistic jets) are the same (Zhang and Mészáros 2004).

The closest analogs within the Milky Way galaxy of the stars producing long gamma-ray bursts are likely the Wolf–Rayet stars, extremely hot and massive stars, which have shed most or all of their hydrogen envelope. Eta Carinae, Apep, and WR 104 have been cited as possible future gamma-ray burst progenitors. It is unclear if any star in the Milky Way has the appropriate characteristics to produce a gamma-ray burst.

The massive-star model probably does not explain all types of gamma-rays burst. There is strong evidence that some short-duration gamma-ray bursts occur in systems with no star formation and no massive stars, such as elliptical galaxies and galaxy halos. The favored theory for the origin of most short gamma-ray bursts is the merger of a binary system consisting of two neutron stars. According to this model, the two stars in a binary slowly spiral towards each other because gravitational radiation releases energy (Abbott et al. 2021)until tidal forces suddenly rip the neutron stars apart and they collapse into a single black hole. The in fall of matter into the new black hole produces an accretion disk and releases a burst of energy, analogous to the collapsar model. Numerous other models have also been proposed to explain short gamma-ray bursts, including the merger of a neutron star and a black hole, the accretion-induced collapse of a neutron star, or the evaporation of primordial black holes(MacFadyen and Woosley 1999).

An alternative explanation proposed by Friedwardt Winterberg is that in the course of a gravitational collapse and in reaching the event horizon of a black hole, all matter disintegrates into a burst of gamma radiation (Stephan Meller,1Franziska Winterberg et al 2005)

Strong evidence showed that long gamma-ray bursts are connected to massive stars can be found in the correlation of some long GRBs with supernovae and the speed at which their host galaxies are star-forming. The collapsar concept (MacFadyen and Woosley 1999) proposes that the core of an extraordinarily massive, low-metallicity, quickly rotating star collapses into a black hole in the course of its evolution. This model is the most widely accepted explanation for the formation of long-duration GRBs. A high-density accretion disk is formed as material from the star's vicinity rains down and swirls toward the star's core. When this material falls into a black hole, it creates two relativistic jets that shoot out along the rotating axis and tear through the star envelope before piercing the surface and emitting gamma rays. Although the majority of the other aspects of the model (the collapse of the core of a big star and the generation of relativistic jets) are the same, some alternative models substitute the black hole with a freshly generated magnetar.

The Wolf-Rayet stars, which are extremely hot and massive stars that have lost most or all of their hydrogen envelope, are most likely the Milky Way galaxy's closest analogs to the stars that produce extended gamma-ray bursts. Eta Carinae, Apep, and WR 104 have all been mentioned as potential gamma-ray burst precursors in the future. It is unknown if any Milky Way star possesses the necessary qualities to produce a gamma-ray burst (Stanek et al. 2007).

Probably not all sorts of gamma-ray bursts can be explained by the massive-star concept. Strong evidence suggests that some short-duration gamma-ray bursts can be found in environments like elliptical galaxies and galactic halos that lack large stars and star formation. The merger of a binary system made up of two neutron stars is the most popular idea for the cause of most brief short gamma-ray bursts. According to this theory, a binary of two stars steadily spirals towards one another due to the release of energy via gravitational radiation (Abbot 2008), until tidal forces suddenly tear the neutron stars apart, causing them to merge into a single black hole. Similar to a collapsar, the infall of matter into the nascent black hole creates an accretion disk and unleashes a burst of energy.

Friedward Winterberg put out the idea that all stuff is converted into a burst of gamma radiation during a gravitational collapse and as it approaches the event horizon of a black hole.

2.3 Long and Short Gamma-Ray Burst

The launch of the Swift satellite has opened a new era of gamma-ray burst (GRB) studies(Perna, Armitage, and Zhang 2006). The apparent separation between Short Gamma ray Burst SGRBs and Long Gamma ray Burst LGRBs, discovered in the GRB population detected by BATSE/ Compton Gamma Ray Observatory (CGRO, was confirmed by HETE-2, Beppo Satellite per Astronomic X (Beppo SAX, Integra Swift and Fermi. However, the comparison of the duration distributions of bursts detected by different instruments suffers from instrumental biases induced by the energy range where they operate, the trigger method and the energy range where the T_{90} is computed (on average a smaller T_{90} is estimated with light curves of higher energy photons.

A new phase in the study of gamma-ray bursts (GRBs) has begun with the launch of the Swift spacecraft (Perna, Armitage, and Zhang 2006). It was confirmed by HETE-2, Beppo Satellite per Astronomic X (Beppo SAX), Integra Swift, and Fermi that the apparent separation between Short Gamma Ray Bursts (SGRBs) and Long Gamma Ray Bursts (LGRBs), found in the GRB population identified by BATSE/Compton Gamma Ray Observatory (CGRO), existed. The energy range in which they operate, the trigger method, and the energy range in which the T_{90} is computed all introduce instrumental biases that make it difficult to compare the duration distributions of bursts detected by various instruments (on average, a smaller T_{90} is estimated with light curves of higher energy photons).

Gamma ray bursts (GRBs), which can be generically categorized as either long or short depending on burst duration, are unique, much like fingerprints. Short bursts last less than 2 seconds and can end in just a few milliseconds, but long bursts are more frequent and can continue anywhere from 2 seconds to several minutes. More highly energetic (hard) gamma rays are typically present in short bursts than long bursts. In contrast to long bursts, when the energy conversion seems to remain constant during the burst, it also appears that the energy conversion into gamma rays diminishes as the burst develops.

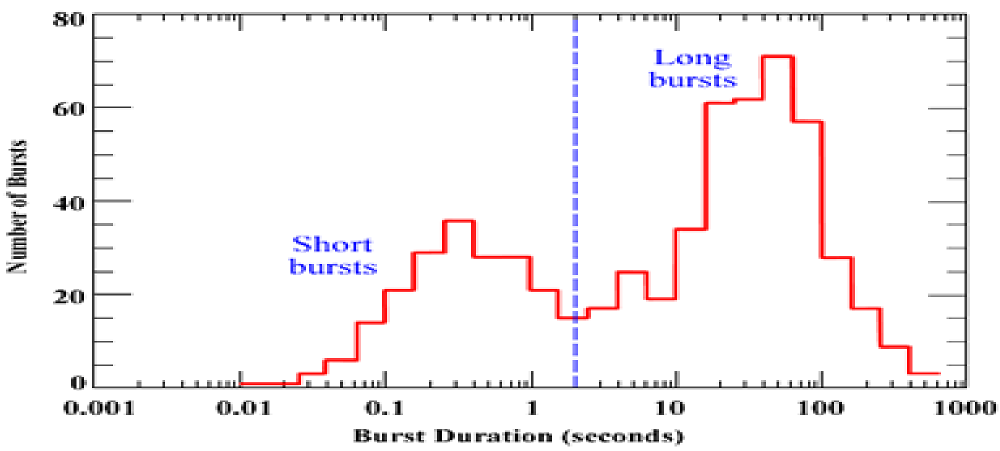

Figure 2.1: Long and short GRB under comparison with their burst duration of time in second(R Perna, PJ Armitage, B Zhang 2006).

If we count the number of GRBs with a particular burst duration, two main populations of GRB emerge. Short bursts have durations of less than 2 seconds, while long bursts last for longer periods. With the most recent sample of GRBs from the GBM/Fermi catalog, we further test these findings. We chose all GRBs that had time-integrated spectra that were well-fit by a Band function or a power law with exponential cutoff. These GRBs were all discovered by the GBM on board Fermi. The red and blue colors in Figure (fig. 2.1) represent the population of short and long events, respectively, which are thought to separate the sample at 2 second. For the two populations, the Kolmogorov- Smirnov (K-S) test probability of E_{peak} and are 10-30 and 10-24%, respectively Additionally, it is confirmed that if the short/long divide is 2 seconds, as has been predicted, collapsars (long GRB progenitors) may contaminate the population of short events, and that the separation between the two classes may be 2 seconds (e.g., 0.8 for Swift). We discover that the K-S probability remains extremely significant of the diversity of the spectral parameters of the two classes even after shifting the long/short division by a factor of two.

It has been discovered that SGRBs are generally harder than LGRBs, providing more evidence that the two populations derive from distinct physical sources. Later, GRB localizations and host identifications were made possible by measurements of the afterglow. These findings provided additional evidence in favor of the multiple source's theory. While SGRB hosts comprise both star-forming and non-star-forming galaxies, LGRB hosts have a high star formation rate. The position distribution of SGRBs inside their hosts is more widespread and appears to have less association with star formation, in contrast to the position distribution of LGRBs within their hosts, which is toward the center and within high star-forming regions. These observations have made it clear that GRBs originate from two distinct progenitors and at least two distinct mechanisms. Recently, it was established that a third mechanism produces low luminosity GRBs. This is distinct from both conventional non-Collapsar short GRBs and Collapsars. They make up a third physical category as a result. Very few bursts are found in the third group of low-luminosity GRBs, and the subject at hand is unrelated to their occurrence. This split is based on various physical mechanisms; thus, it is important to distinguish this third group of low-luminosity GRBs from the hypothetical intermediate group proposed by phenomenology.

The correlation between LGRBs and star-forming areas, as well as their frequent coexistence with Type Ic SNe, points to the possibility of stellar collapse. According to the Collapsar hypothesis, the central engine of the collapsing star, which is most likely propelled by an accretion disk onto a newly created compact object or by a magnetar- powers a jet that pierces the stellar envelope and, once it is outside the star, emits the observed gamma-rays. Typically, weaker and visible at closer ranges, LGRBs. SGRB are more difficult to find. SGRBs are less frequently observed than LGRBs. The SGRBs with locations known are linked to a variety of stellar population ages. Although the precise origin is yet unknown, their features are compatible with those expected from binary neutron star mergers.

The observed groups of LGRBs and SGRBs and the astrophysical groups of Collapsars and non-Collapsars are often implicitly thought to correlate one-to-one. There is a large overlap between the two categories of long and short GRBs, according to a brief examination of the duration distribution, which reveals that some SGRBs have Collapsar origins and others have long GRBs. The only notable difference between LGRBs and SGRBs in terms of high-energy emission qualities is a little variation in average hardness. This makes it challenging to pinpoint the source of any given burst, and in the absence of a better standard, the original division according to $T_{90} \lesseqgtr 2$ sec is frequently employed. However, this standard was developed for a particular detector (BATSE) and a particular observing window. Since SGRBs are often tougher than LGRBs, softer detectors like Swift/BAT have a harder time picking them up than BATSE. When the criterion $T_{90} \lesseqgtr 2$ sec is applied, Swift's short/long detection rate is 1/10 compared to BATSE's 1/3. In fact, a visual examination of Swift's duration distribution reveals that the division line between the two groups may be at a lower duration as a result of this (Norris and Bonnell 2006).

3 Data and Methodology

The redshift distribution of gamma-ray bursts (GRBs) is calculated assuming that they trace the cosmic star formation history. Based on the complete GRB sample, we directly construct the GRB luminosity function and redshift distribution in the frameworks of different evolution models using the maximum likelihood method that performs an analysis for the redshift and luminosity distributions of the GRB sample and the Monte Carlo technology that provides the best-fitting parameters and the probability density distributions of the parameters in each model.Analysis method a maximum likelihood method firstly introduced by Marshall et al. (1983) (GX Lan, JJ Wei, HD Zeng, Y Li 2021) is adopted in our analysis. The model free parameters can be optimized by maximizing the likelihood function. Using the maximum likelihood analysis method, we can optimize the values of free parameters of the GRB luminosity function. For the graphs and plots of the result, we have used Microsoft excel 2021, OriginPro 2019b and Statistical Package for the Social Sciences (IBM SPSS Statistics v26 2019) softwares. Integrations and derivatives were done by the ExceLab 365.

3.1 Luminosity Function of Gamma-Ray Burst

The number of bursts per luminosity unit is how the GRB luminosity function is typically characterized. The original idea behind the luminosity function was inspired by astronomical objects like galaxies and stars, which are steady and long-lasting in terms of emitting energy. For GRB-like high energy transients, the total isotropic-equivalent energy (E_{iso}) released over the course of one event can be accurately measured. Additionally, its function (i.e., the number density of bursts per E_{iso} interval) probably offers an independent or even more significant hint on the underlying physics (Xu 2022).

The number of GRBs recorded as a function of measurably defined parameters is an interesting estimable quantity for any gamma-ray burst (GRB) detector. This is dependent on both the measured GRB production rate and the distribution of GRB intrinsic features, as well as instrumental parameters like the duration of operation, T, and field of view. Using the formalist approach described (Tan, Cao, and Yu 2013). Most generally, the number of GRBs detected by the instrument in the luminosity (L) range $L_1$to L_2 and redshift range $z_1$to z_2 is given by

$$N\ (L_1, L_2;\ z_1\ , z_2)\ =\ T\frac{\Delta\Omega}{4\pi}\int_{L_1}^{L_2}\phi\ (L)dL\int_{z_1}^{z_2}\frac{\dot{R}(z)}{1+z}dv \qquad 3.1$$

The function $\phi(L)$ is formally called the 'luminosity function (LF) having units of $(erg\ s^{-1})^{-1}$, ΔΩ is the field of view of the detector of GRB. In view of the fact that GRBs are end-products of massive stars in galaxies, the GRB formation rate $\dot{R}(z)$ can be written

$$\dot{R}(z) = f_b C\dot{\rho}_* \qquad 3.2$$

$$C = \frac{E_\gamma}{E_\gamma + E_k} \qquad 3.3$$

Where E_γ is the isotropic equivalent energy of the γ-ray emission and E_k is the isotropic equivalent energy of the outflow powering the afterglow. Following the Swift observations of in the X-ray afterglow light curve of many GRBs, it has been argued that typical values of C could be as high as 90 percent or even higher (Y Fan, T Piran 2006). Where $\dot{\rho}_*$ gives the cosmic star-formation rate (CSFR) in $M_\odot\ Gpc^{-3}yr^{-1}$, C gives the efficiency of GRB production given a certain stellar mass, in units of $M_\odot\ ^{-1}$, and f_b encodes the beaming effect of the relativistic jets producing the burst. All of these terms may be functions of the redshift(Paul 2018).

Table 3.1: GRB energies and efficiencies(Fan, Y., & Piran, T 2006)

GRB	Eγ	Ek	C (efficiency)
970228	1.42	17.5	0.08
970508	0.55	9.1	0.06
970828	21.98	37.4	0.37
971214	21.05	78	0.21
980613	0.54	11.2	0.05
980703	6.01	22.2	0.21
990123	143.8	186.6	0.43
990510	17.6	121.1	0.13
990705	25.6	3.1	0.89
991216	53.5	337.1	0.14
000216	16.9	4.6	0.78
000926	27.97	91.7	0.23
010222	85.78	209.7	0.29
011211	6.72	12.1	0.36
020405	7.2	42.3	0.15
020813	77.5	203.9	0.28
021004	5.56	76.8	0.07

Two key properties that characterize the population of GRBs are (a) cosmic rate of Gamma-Ray Burst formation rate, $\dot{R}(z)$ representing the number of bursts per unit comoving volume and time as a function of redshift, and (b) their luminosity function ϕ(L) (LF), which represents the relative fraction of bursts with a certain luminosity.

GRBs are very changeable objects, hence defining a brightness requires defining a temporal period. The luminosity function is typically studied using measurements of average brightness (total isotropic energy divided by cosmic rest-frame time) and peak luminosity. The luminosity at the peak of a burst is known as the peak luminosity. In order to provide an accurate measurement, one must, in theory, define the same unit time interval in the rest frame for each GRB. In reality, one typically determines the peak flux using the detector's energy band for a specific time bin in the observer frame because some GRBs do not have redshift data (e.g., 64 ms or 1 s). Generally, LF of GRBs can be expressed by the Schechter function as follows:

$$\phi(L) \; = \; A\left(\frac{L}{L_*}\right)^{-\alpha} \exp\,(\frac{-L}{L_*})\,\frac{1}{L_*} \qquad 3.4$$

Where L is the isotropic-equivalent peak luminosity, α is he slope and L_* break luminosity and A is normalization constant and is equal to $1/\int_0^\infty \phi(L)dL$. This functional form has the advantage of having only 3 parameters: the isotropic-equivalent peak luminosity L, the break luminosity L_* and the slope α. The isotropic-equivalent peak luminosity in the source frame can be calculated as

$$L = 4\pi D_L(z)^2 P \frac{k(z)}{w} \quad 3.5$$

$$D_L = c(1+z)\int_0^z \frac{1}{H(z')}dz' \quad 3.6$$

$$H(z') = H_0[(1+z)^3\Omega_m + \Omega_\Lambda + (1-\Omega_m) + (1+z)^2]^{1/2} \quad 3.7$$

where P is the peak flux in the observed energy band of 15 -150 keV of swift onboard BAT satellite. The term k(z)/w is to convert the observed energy band to the rest frame band of 1-10^4 keV. Here c accounts for the bolometric energy fraction that seen in the detector band (Wanderman & Piran 2010, Howell et al. 2011), and k(z) is the cosmological correction. We express them in the form of

$$k(z) = \int_{15kev}^{150kev} ES\,(E)dE \int_{15(1+z)}^{150(1+z)} ES\,(E)dE \quad 3.8$$

$$w = \int_{15kev}^{150kev} ES\,(E)dE \int_1^{10^4} ES\,(E)dE \quad 3.9$$

Here S (E) is the rest frame photon spectrum, which can be well expressed by the empirical Band function (Band et al.2003). The high and low energy spectral indices are given by -2.25 and -1, respectively. The spectral peak energy in the source frame can be described as follows

$$E_p = \frac{(2+\alpha)E_o}{\alpha-\beta} \quad 3.10$$

Where E_o the break energy having value of 100 Kev.

When the detector's energy band is wide enough, a GRB spectrum can usually be fit with a smoothly joint (in an exponential form) broken power law known as the Band function or GRB function (Preece et al. 2000). The photon number spectrum in this model reads:

$$S(E) = \begin{cases} A\left(\frac{(\alpha-\beta)\,E_o}{100KeV}\right)^{(\alpha-\beta)} exp\,(\alpha-\beta)\left(\frac{E}{100KeV}\right)^{\beta} & E \geq (\alpha-\beta)\,E_o \\ A\left(\frac{E}{100KeV}\right)^{\alpha} \exp\left(-\frac{E}{E_o}\right) & E < (\alpha-\beta)\,E_o \end{cases} \quad 3.11$$

Following the definitions and notation (Bloom et al.2003), the value for E_γ, the total prompt energy release in a certain bandpass, may be found from:

$$E_\gamma = S_\gamma \frac{4\pi {D_L}^2}{1+z} k f_b \quad 3.12$$

where S_γ is the fluence (The fluence of gamma-ray bursts (GRBs) are measured with a variety of instruments in different detector energy ranges) received in some observed bandpass and D_L is the luminosity distance at redshift z. The quantity k is a multiplicative correction of order unity relating the observed bandpass to the standard rest frame-bandpass(Bloom, Frail, and Kulkarni 2003), and f_b is the beaming factor(1-cosθ_j) and $\frac{dV}{dz}$ is the comoving volume element per unit redshift, given by

$$\frac{dV}{dz} = \frac{4\pi c {D_L}^2}{H(z)} \frac{1}{(1+z)^2} \quad 3.13$$

The luminosity distance, D_L to the source at redshift, z

$$D_L = c(1+z)\int_0^z \frac{1}{H(z')} dz' \quad 3.14$$

$$H(z') = H_0[(1+z)^3\Omega_m + \Omega_\Lambda + (1-\Omega_m) + (1+z)^2]^{1/2} \quad 3.15$$

Ω_m and Ω_Λ are the dimensionless matter density and dark energy density parameters of the universe, respectively and c is speed of light.

$$R(z) = \frac{R_{GRB}}{1+z} \frac{dV(z)}{dz} \quad 3.16$$

is the differential comoving rate of bursts at a redshift z, $\frac{dV(z)}{dz}$ is the derivative of the volume element and the factor 1/ (1 + z) reflects the cosmological time dilation and

$$\frac{dV}{dz} = \frac{4\pi c {D_L}^2}{H(z)} \frac{1}{(1+z)^2} \quad 3.17$$

as described in equation (Eq 3. 16) R_{GRB} is defined as GRBs formation rate in the interval z to z + dz. Since long GRBs are very likely related to the death of massive stars, the simplest assumption is to adopt a GRB rate proportional to the SFR. Here we are going to use the method of Porciani and Madau to find the comoving rate of GRB as follows;

$$R_{GRB} = \mathrm{k} \times R_{SN} \qquad 3.18$$

Where k is the free parameter of the model.

Where $\dot{R}(z)$ is the GRB comoving rate and R_{SN} is the Type II supernova comoving rate. We assume the same initial mass function constant with time, the supernovae rate is proportional to the SFR:

$$R_{SN}(\mathrm{z}) = 0.0122\, M_{\odot}^{-1} \times R_{SF}(\mathrm{z})_{(1,2,3)} \qquad 3.19$$

$$\frac{\int_{m_c}^{m_u} dm\phi(m)/m}{\int_{0}^{m_u} dm\phi(m)} = 0.0122\, M_{\odot}^{-1} \qquad 3.20$$

Where ϕ(m) is the initial mass function (IMF) of stars, for which we take the Salpeter form ϕ (m), $m_u = 125M_{\odot}$ and m_c= critical mass for Type II supernovae m_c to be between 8 and 10 $M_{\odot}$ according to Nomoto (1984).

First it is better to look at the SFR at different intervals of the redshift.

$$R_{SF}(\mathrm{z})_{(1)} = 0.3h_{70} \frac{\exp(3.4z)}{\exp(3.8z)+45}\, M_{\odot}\, yr^{-1}Mpc^{-3} \qquad 3.21$$

The SFR increases rapidly between z = 0 and 1, peaks between z= 1 and 2, and gently declines at higher redshifts. Because of the uncertainties associated with the incompleteness of the data sets and the amount of dust extinction at early epochs, we consider a second scenario in which the SFR instead remains roughly constant at z $\geq$ 2 (Steidel et al. 1999).

$$R_{SF}(\mathrm{z})_{(2)} = 0.15h_{70} \frac{\exp(3.4z)}{\exp(3.4z)+22}\, M_{\odot}\, yr^{-1}Mpc^{-3} \qquad 3.22$$

Some recent studies have suggested that the evolution of the SFR up to z = 1 may have been overestimated (Cowie, Songaila, & Barger 1999), while the rates at high z may have been severely underestimated due to large amounts of dust extinction (Blain et al. 1999). We then consider a third SFR,

$$R_{SF}(z)_{(3)} = 0.2h_{70}\frac{\exp(3.05z-0.4)}{\exp(2.93z)+15}\ M_{\odot}\,yr^{-1}Mpc^{-3} \quad 3.23$$

with more star formation. Assuming that all stars with masses M > 8 $M_{\odot}$ explode as core-collapse supernovae (SNe), the SN II rate density $R_{SN}(z)$ can then be estimated by multiplying the selected SFR by the coefficient.

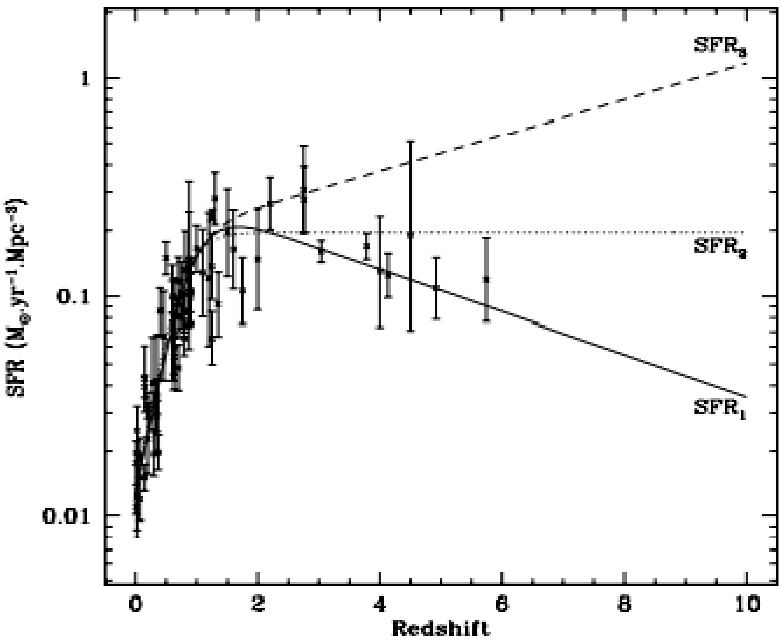

Figure 3.1: The three-star formation rates. Observed data are taken from Hopkins (2004)

$$R_{GRB} = k \times 0.0122\ M_{\odot}^{-1} \times R_{SF}(z)_{(1,2,3)} \quad 3.24$$

According to the information above, Porciani & Madau's method of calculating the star formation rate suggests three parameterized versions of the SF rate that are very similar at low redshifts but different at high redshifts, where the interpretation of the data is unclear due to the poorly understood effects of dust absorption. In order to determine the star formation rate of Gamma-Ray Burst as a function of redshift, it is preferable to take into consideration an alternative way as follows; At large redshifts, it is difficult to forecast SFR by the aforementioned formalism of Porciani and Madau's work.

$$R_{SF}(z) = \frac{0.15e^{3.14z}}{22+e^{3.14z}} M_{\odot}\,yr^{-1}Mpc^{-3} \quad 3.25$$

This expression describes a constant SF rate at large redshifts (Stern, Atteia, and Hurley 2002).

3.2 Fluence of Gamma-Ray Burst

The total energy released by a gamma ray burst during its active gamma ray phase is recorded as the fluence of the burst. This corresponds to the flux integrated over the duration of the burst, and ranges over magnitude approximately from 10^{-8} to 10^{-3} erg/cm^2. The fluences of GRB is the amount of energy received over the time duration of the GRB(Nava et al. 2008). The peak fluence of GRB can be found as follows

$$S_E^P = \frac{L_{iso}^E}{4\pi {D_L}^2(z)(1+z)} T \qquad 3.26$$

Where S_E^P *is* the bolometric Fluence, L_{iso}^Eisotropic peak Luminosity (in erg/second) of GRB, T is the time of trigger of GRB and z the redshift. The above formula did not give the observed peak fluence and the peak fluence can be calculated as follows;

$$S_E^{P,obs} = \int ES\left(E, \alpha, \beta, E_{peak}^{obs}, A^*\right) dE \qquad 3.27$$

Where E - Energy band of detector, α andβ are the lower and upper index

E_{peak}^{obs} − observed peak energy of the band

A^* − is the normalization constant

3.3 Flux of Gamma-Ray Burst

There are generally three spectral shape parameters available for each spectrum: a low-energy power-law index,α, a characteristic break energy, and possibly a high energy power-law index,β. The observed photon flux, P, in the energy band $E_{min} < E < E_{max}$ emitted by an isotropically radiating source at redshift z is

$$F = 1 + z \frac{\int_{(1+z)E_{min}}^{(1+z)E_{max}} S(E) dE}{4\pi {D_L}^2(z)} \qquad 3.28$$

$$S(E) = \begin{cases} A\left(\frac{(\alpha-\beta)\, E_{Peak}}{100KeV}\right)^{(\alpha-\beta)} exp\,(\alpha-\beta)\left(\frac{E}{100KeV}\right)^{\beta} & E \geq (\alpha-\beta)\, E_{peak} \\ A\left(\frac{E}{100KeV}\right)^{\alpha} \exp\left(-\frac{E}{E_{Peak}}\right) & E < (\alpha-\beta)\, E_{Peak} \end{cases} \qquad 3.29$$

Where, $S(E)$ (Xu 2022) is the differential rest-frame photon luminosity of the source and D_L is the of luminosity distance. To describe the typical burst spectrum, we adopt the functional form proposed by Band et al. (1993), i.e., a broken power law with a low energy spectral index α, a high-energy spectral index β, and a break energy E_b . In this work, we take α= -1, β = 2.25 (Preece et al. 2000), and $E_b = 511$ keV. The isotropic equivalent intrinsic burst luminosity in the energy band 30–2000 keV as L = $\int_{30kev}^{2000kev} ES(E)dE$. Given a normalized GRB Luminosity Function $\phi(L)$ and detector efficiency $\epsilon(P)$, the observed rate of bursts with peak flux P between P_1 and P_2 is

$$\frac{dN}{dt}(F_1 < F < F_2) = \int_0^{\infty} (dz \frac{dV(z)}{dz} \frac{\Delta\Omega_s}{4\pi} \frac{R_{GRB}}{1+z}) \times \int_{F,z}^{F_2,z} dL' \phi(L')\, \epsilon(P) \qquad 3.30$$

$\frac{dV(z)}{dz}$ is the comoving volume element and $\Delta\Omega_s$ is the solid angle covered on the sky by the survey, and the factor $\frac{1}{1+z}$ accounts for cosmological time dilation and finally R_{GRB} is the gamma-ray burst formation rate. We consider the GRB formation rate is proportional to rate of type II supernova R_{SN},

$$R_{GRB} = k \times R_{SN} \qquad 3.30$$

We can then calculate the peak fluxes in erg $cm^{-2}s^{-1}$ as follows

$$F_E^P = \frac{L_{iso}^E}{4\pi {D_L}^2(z)(1+z)^2} \text{ erg } cm^{-2}s^{-1} \qquad 3.31$$

However, the above equation gives the bolometric value of flux, not observed flux; to calculate the observed peak flux, we must model the instruments parameters such as E_{iso}, E_{Peak} and z(redshift) from the simulations, and calculate the normalization constant A* of the Band function. We can calculate the observed peak flux as follows

$$S_E^{P,obs} = \int EN\left(E, \alpha, \beta, E_{peak}^{obs}, A^*\right) dE \qquad 3.32$$

$$N(E) = A(E/100Kev)^{\alpha} \exp(-E/E_{Peak}) \text{ for } E < (\alpha - \beta)\, E_{Peak} \qquad 3.33$$

Then $$F_E^{P,obs} = \frac{S_E^{P,obs}}{T(1+Z)} \qquad 3.34$$

$S_E^{P,obs}$ is the observed peak fluence of detectors of Gamma-Ray Burst.

3.4 The Redshift of Gamma-Ray Burst

The spectral lines that we see from a single star in the Galaxy do not have wavelengths that are exactly the same as those lines that we see in the lab. Depending on how fast the star is moving in relation to the Earth, the lines are systematically moved either to the red or to the blue. The total relative velocity is the sum of the Earth's rotational velocity, the Earth's velocity around the Sun, the Solar System's velocity around the Galaxy's center, and any star's velocity(Le and Mehta 2016). A different part of the redshift would relate to the universe's expansion in the most recent cosmological models. According to these ideas, if the universe is expanding, as predicted by general relativity, then spacetime must also be expanding. This causes a change in the Rydberg constant, which results in a redshift, as well as a dilating of wavelengths and a concomitant contraction of frequencies. Every point in space and every direction in space experience the same rate of expansion (homogeneity) and isotropy, respectively, in the universe (V Dániel, A Inneman, L Pína, V Zadražil).

The shifts in a frequency of light emitted by distant sources provide us with the most crucial information about the cosmic scale factor R(t), which indicates the relative expansion of the Universe and can be used to measure both the distance and the time in the universe. We will start by locating ourselves at the coordinate system's origin, r = 0, to determine this frequency shift (according to cosmological principle). From the typical signal it is found that

$$\frac{\delta t_0}{R(t_0)} = \frac{\delta t_1}{R(t_1)} \quad 3.35$$

The frequency emitted (v_0) is related to the frequency observed (v_1) by

$$\frac{v_0}{v_1} = \frac{\delta t_1}{\delta t_0} = \frac{R(t_1)}{R(t_o)} \quad 3.36$$

This is conventionally expressed in terms of redshift parameter z, defined as the fractional increase in wavelength

$$z = \frac{\lambda_o - \lambda_1}{\lambda_1} \quad 3.37$$

$$\text{Since } \frac{\lambda_o}{\lambda_1} = \frac{v_1}{v_0} \text{ then } z = \frac{R(t_0)}{R(t_1)} - 1 \quad 3.38$$

To avoid confusion, it should be kept in mind that υ_1 and λ_1 are frequency and wavelength of observed near the place and time of emission, and hence presumably take the value measured when the same atomic transition occurs in terrestrial, while υ_0 and λ_o are the frequency and wavelength of light observed after its long journey to us. If $z > 0$ then $\lambda_o > \lambda_1$ and we speak of redshift; if $z < 0$ the $\lambda_o < \lambda_1$ and we speak of a blue shift. If the universe is expanding, then $R(t_0) > R(t_1)$ and equation (2.37) gives a redshift, while if the universe contracting, then $R(t_0) < R(t_1)$ and equation (3.37) gives a blueshift. Such frequency shift finds a natural explanation of the Doppler effect.

Using absorption lines, photometry, the optical afterglow spectrum, or the emission lines in the spectrum of the host galaxy, one can determine the redshifts of GRBs. However, for the three separate detection methods-absorption, emission, and photometry-we observe distinct redshift distributions in the global sample. We do not observe high-redshift events for redshifts calculated from the hosts' emission lines, but absorption line redshifts cover the complete range of redshifts (Wanderman and Piran 2010).

Table 3.2: Gamma-Ray Burst data taken from National Aeronautics and Space Administration Goddard Space Flight Center on swift BAT satellite for further analysis

GRB	Trigger number	Right Accretion (RA	Declination (Dec)	T_{90} in second	fluence	index	redshift
22017A	1093611	91.59	-28.408	49.81	16	1.84	4.961
220101A	10991527	1.360	13.785	173.36	250	1.13CPL	4.61
211207A	1088376	196.601	-24.360	3.75	1.9	1.72PL	2.272
211024B	1081073	154.708	24.506	603.5	68	1.63	1.113
211023B	108085	170.314	39.133	1.30	1.7	1.7PL	0.862
210822A	106988	304.46.	5.265	180.80	200	1.7PL	1.73
210731A	1062336	300.311	-28.056	22.51	22	0.25CPL	1.2525
210722A	1061223	27.03	-6.347	50.20	25	1.6PL	1.445
210619B	1050757	319.718	33.85	60	950	1.14PL	1.937
210610B	1054885	243.929	14.398	69	38	0.98CL	1.13
210610A	1054627	204.284	14.476	13.62	10	1.14PL	3.54
210517A	1048783	358.19	-39.104	3.06	1.5	1.65	2.468
210504A	1034543	222.379	-30.557	135.06	27	1.64PL	2.077
210420B	1044382	254.313	42.558	158.8	15	1.49PL	1.4
210411C	1042398	296.601	39.399	12.80	12	1.692PL	2.826
210321A	1037828	87.887	70.109	8.21	6.7	2.15PL	1.487
210222B	1034325	154.631	-14.946	12.82	3.4	2.37PL	2.198
210210A	1031728	262.764	14.657	6.60	9.8	1.35CPL	0.157
201221D	1014037	171.055	42.152	0.16	3.9	1.56PL	1.046
201221A	1013852	214.488	-45.406	44.5	18	1.4PL	5.70
201104B	1004168	5.215	7.834	8.66	18	1.47PL	1.95
201024A	1001514	125.959	357	5	8.1	2.10PL	0.999
201021C	10001130	12.503	-55.862	24.38	10	1.63PL	1.070
200205B	954519B	107.760	-56.488	458	54	1.36CPL	1.465
190719C	195381	240.208	13.005	185.7	51	1.64PL	2.649
181020A	867987	13.987	-47.372	238	81	1.25PL	2.938
171205A	794972	167.423	-12.599	189.4	36	1.45PL	0.368

Fluence (10^{-7} erg/cm^2 (15-150 keV); flux (ph/cm^2/sec (15-150 keV); PL = simple power-law, CPL = cutoff power-law (15-150 keV)

Taking into account the above data of redshift, we are going to calculate the expected redshift distribution of GRBs as follows:

$$\frac{dN}{dz} = F(z)\frac{\varepsilon(z)R_{SF}}{f_{beam}}\frac{dV_{com/dz}}{1+z} \quad 3.39$$

$$f_{beam} = 1 - cos\theta_j \quad 3.40$$

$$\text{If} \quad \theta_j \leq 1, f_{beam} = \frac{\theta_j{}^2}{2} \qquad 3.41$$

Where, θ_j is the opening angle of Gamma-Ray Burst, , ε(z) accounts for the fraction of stars producing GRBs, and F(z) can be treated as constant when we consider the bright bursts with luminosities sufficient to be detected within an entire redshift range and so $0<F(z)<1$ where summarizes the ability both to detect the initial burst of gamma rays and to obtain a redshift from the optical afterglow and includes observational factors such as instrumental sensitivities (Al 2008).

Beaming rendering some fraction of GRBs unobservable from Earth is accounted for through $f_{beam}.\frac{1}{1+Z}$ the is due to cosmological time dilation of the observed rate, and dV/dz is the comoving volume per unit redshift. The ε(z) can be parameterized as $\varepsilon(z) = \varepsilon_0 \ (1 + z)^{\delta}$, where ε_0 is an unknown constant that includes the absolute conversion from the SFR to the GRB rate in a given GRB luminosity range or reflects the fraction of stars that produce long-duration GRBs and any additional evolutionary effects. Kistler et al. (2008) find the index δ(enhanced evolution of gamma ray burst) = 1.5 from 63 Swift GRBs(F. Y. Wang 2013).

Table 3.3 : The beaming factor of Gamma-Ray Burst from swift satellite(Frail et al.)

GRB	θ_j	F_{beam}
970508	0.293	0.042925
970828	0.072	0.002592
971214	0.056	0.001568
980613	0.127	0.008065
980703	0.135	0.009113
990123	0.05	0.00125
990510	0.053	0.001405
990705	0.054	0.001458
990712	0.411	0.084461
991208	0.079	0.003121
991216	0.051	0.001301
000131	0.047	0.001105
000301C	0.105	0.005513
000418	0.198	0.019602
000926	0.051	0.001301

Table 3.4: Data of GRB taken directly from National Aeronautics and Space Administration Goddard Space Flight Center on swift 4B with known values of quantities.

GRB	Fluence 10^{-7} erg/cm^2	Peak flux ph/cm^2 s	Redshift (z)	Log $D_L(z)$	E_{iso} 10^{51} erg	L_{iso} 10^{58} ph/s
050126	8.38	0.71	1.29	9.12	3.60	0.31
050223	6.36	0.69	0.588	3.44	0.57	0.061
050315	32.2	1.93	1.949	15.24	30	1.80
050318	10.8	3.16	1.44	10.46	5.80	1.70
050319	13.1	1.52	3.24	28.37	30	3.50
050401	82.2	10.7	2.9	24.81	160	20
050505	24.9	1.85	4.27	39.49	88	6.60
050525A	153	41.7	0.606	3.57	15	4.00
050603	63.6	21.5	2.821	23.99	110	39
050724	9.98	3.26	0.258	1.29	0.16	0.052
050730	23.8	0.55	3.969	36.2	75	1.70
050802	20	2.75	1.71	12.96	15	2.00
050803	21.5	0.96	0.422	2.3	0.96	0.04.3
050814	20.1	0.71	5.3	50.99	99	3.50
050820A	34.4	2.45	2.613	21.85	54	3.90
050824	2.66	0.5	0.83	5.26	0.48	0.090
050826	4.13	0.38	0.297	1.52	0.088	0.0081
050904	48.3	0.62	6.195	61.22	300	3.90
050908	4.83	0.7	3.346	29.49	12	1.70
051016B	1.7	1.3	0.396	6.11	3.90	3.00
051109A	22	3.94	2.346	19.15	2.90	5.20
051109B	2.56	0.55	0.08	0.36	0.0037	0.00078
051111	40.8	2.66	1.549	11.46	25.0	1.60
060108	3.69	0.77	2.03	16.03	3.70	0.78
060115	17.1	0.87	3.53	31.45	45	2.30
060123	3	0.04	1.099	7.47	0.95	0.013
060124	4.6	0.89	2.298	18.67	5.80	1.10
060210	76.6	2.72	3.91	35.55	3.60	8.40

GRB	Fluence 10^{-7} erg/cm^2	Peak flux ph/cm^2 s	Redshift (z)	Log D_L(z)	E_{iso} 10^{51} erg	L_{iso} 10^{58} ph/s
060218	15.7	0.25	0.033	0.14	0.0037	0.000059
060222A	6.73	1.35	4.41	41.03	250	5.00
060418	83.3	6.52	1.49	10.91	480	3.70
060502A	23.1	1.69	1.51	11.1	140	0.99
060520A	9.44	2.65	0.089	0.4	0.017	0.0047
060510B	40.7	0.57	4.9	46.49	1800	2.50
060512	2.32	0.88	0.443	2.44	0.11	0.043
060522	11.4	0.55	5.11	48.85	53	2.60
060526	12.6	1.67	3.21	28.05	28	3.70
060622A	16.1	0.56	0.787	4.92	2.60	0.091
060614A	4.02	0.34	2.68	22.54	6.60	0.56
060615	6.97	0.46	3.76	33.93	20	1.3
060617A	25.5	1.4	3.082	26.71	53	2.90
060614B	204	11.5	0.128	0.59	0.76	0.043
060719	16	1.01	3.43	30.39	40	2.50
060713	28.3	1.28	2.71	22.84	48	2.20
060729	26.1	1.17	0.54	3.1	1.90	0.087
060814C	1 146	7.27	0.84	5.34	27	1.30
060914B	16.2	2.44	0.703	4.28	2.10	0.31
060916	22.1	1.97	3.685	33.12	0.32	5.50
060918	28	3.03	2.43	20	39	4.20
060912	13.5	8.58	0.937	6.12	3.10	2.00
060927	11.3	2.7	5.6	54.4	61	14
061017B	444	14.6	1.262	8.87	180	6.10
061110A	10.6	0.53	0.758	4.7	1.60	0.080
061110B	13.3	0.45	3.44	30.49	33	1.10
061121	137	21.1	1.314	9.33	62	9.50
061210B	11.1	5.31	0.41	2.22	0.47	0.22
061222B	22.4	1.59	3.355	29.59	54	3.80

4 Results and Discussion

The luminosity function of gamma ray burst can be expressed by the Schechter luminosity function as follows by the column graph.

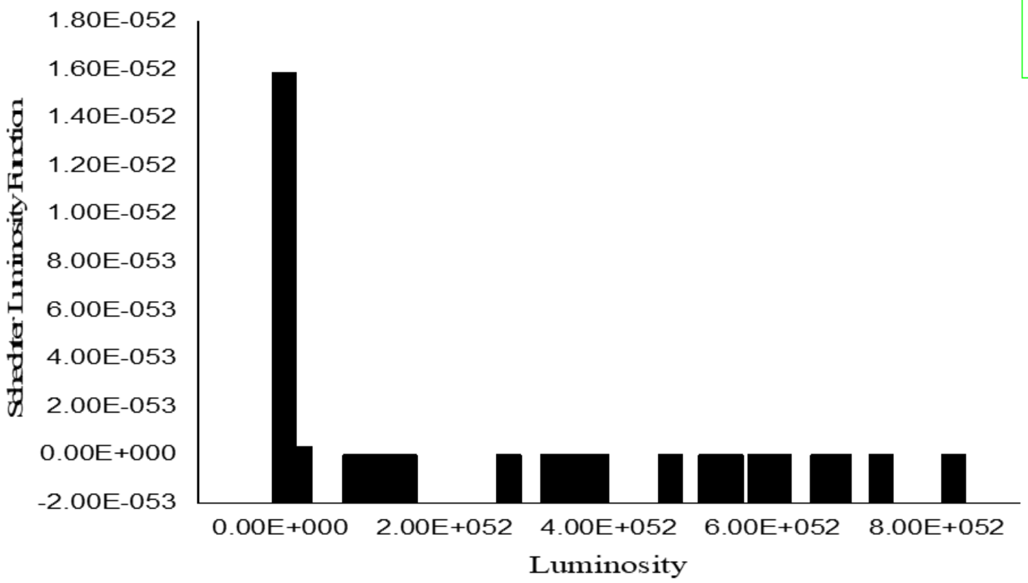

Figure 4.1: The isotropic peak Luminosity vs. the Schechter Luminosity Function

The above graph is based data of isotropic luminosity of GRB taken from table 3.4, and its break luminosity was 511 kev of swift BAT satellite. We have taken the lower exponential idex (α) = -1.5. This Schechter luminosity function is independent of redshift so, it does not evolve with the increase or decrease of the redshift of gamma-ray burst. But it changes with luminosity of the gamma-ray burst as it is function of it. As we understood from the graph, the luminosity is mostly distributed around at the luminosity values of 4.8E+51 ergs/sec and beyond it, the distribution roughly becomes constant.

Now we are going to find the of gamma-ray burst formation rate by relating to the supernovae type II.

$$R_{GRB} = 0.0122\, M_{\odot}^{-1} \times R_{SF}(\mathrm{z})_{(1,2,3)}$$

$$R_{GRB} = \mathrm{k} \times R_{SN}$$

$$R_{SN} = 0.0122\, M_{\odot}^{-1} \times R_{SF}(\mathrm{z})_{(1,2,3)}$$

$$R_{SF}(\mathrm{z})_{(1)} \;= 0.3h_{70}\frac{\exp(3.4z)}{\exp(3.8z)+45}\; M_{\odot}\, yr^{-1}Mpc^{-3}$$

$$R_{SF}(\mathrm{z})(\mathrm{z})_{(2)} \;= 0.15h_{70}\frac{\exp(3.4z)}{\exp(3.4z)+22}\; M_{\odot}\, yr^{-1}Mpc^{-3}$$

$$R_{SF}(\mathrm{z})(\mathrm{z})_{(3)} = 0.2h_{70}\frac{\exp(3.05\mathrm{z}-0.4)}{\exp(2.93\mathrm{z})+15}\; M_{\odot}\, yr^{-1}Mpc^{-3}$$

We are going to evaluate the star formation rate of gamma ray burst based on the data given on table 3.4 (we used redshift data). The above star formation rates are based from Porciani and Madau and we have tried to explain star formation rates of gamma ray burst taking the recent redshift values of the gamma-ray burst swift 4B catalogue.Accordingly, the star formation rates categorized in to three rates indicated by different colors as indicated by figure (fig 4.2) below. Each color indicates different star formation rate, black indicates star formation rate one, the red color indicates star formation rate two and finally the blue color indicates the star formation rate three.

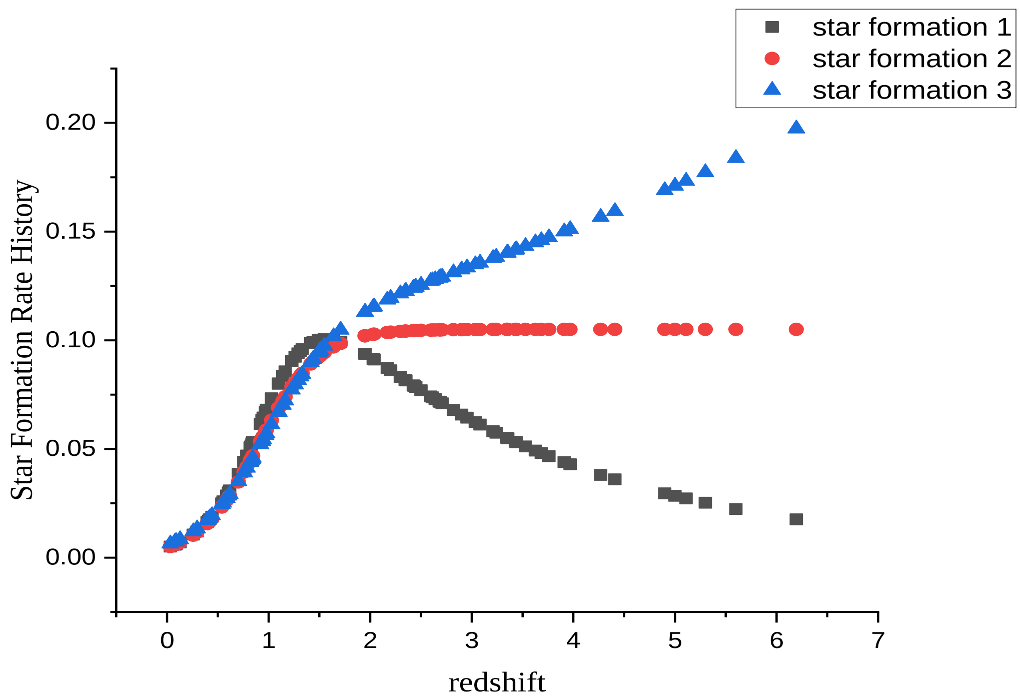

Figure 4.2: The star formation History vs. Redshift of the Gamma-Ray Burst (star formation rate in $M_{\odot}\, yr^{-1}Mpc^{-3}$)

From the above figure (fig 4.2), we understand that, all the star formation rates increase at the beginning to some values of redshift but, it varies after some values of redshift and explained as follows; from star formation rate one (the black color), the star formation rate increases from redshift values of 0.033 to redshift values of 1.549. The star formation rate peaks between z values of 1.49 and 1.549. Above the redshift values of 1.549, the star formation rate decreases rapidly. But according to Nomoto (1984), the SFR increases rapidly between z = 0 and 1, peaks between z= 1 and 2, and gently declines at higher redshifts. Now we are going to look in to star formation rate two (red color), the star formation rate increases from redshift of 0.033 to 1.71 rapidly and from redshift of z value 1.949 to 2.04 increases slowly, and after z values of 2.04 the star formation rate roughly becomes constant. Refer to the star formation rate from scenario in which the SFR remains roughly constant at $z \geq 2$. When referring to star formation rate 3 (blue color), the star formation rate increases starting from z values of 0.033 up to any given values of redshift. From Hopkins (2004) star formation rate three increases starting from zero and increases with increasing of redshift.

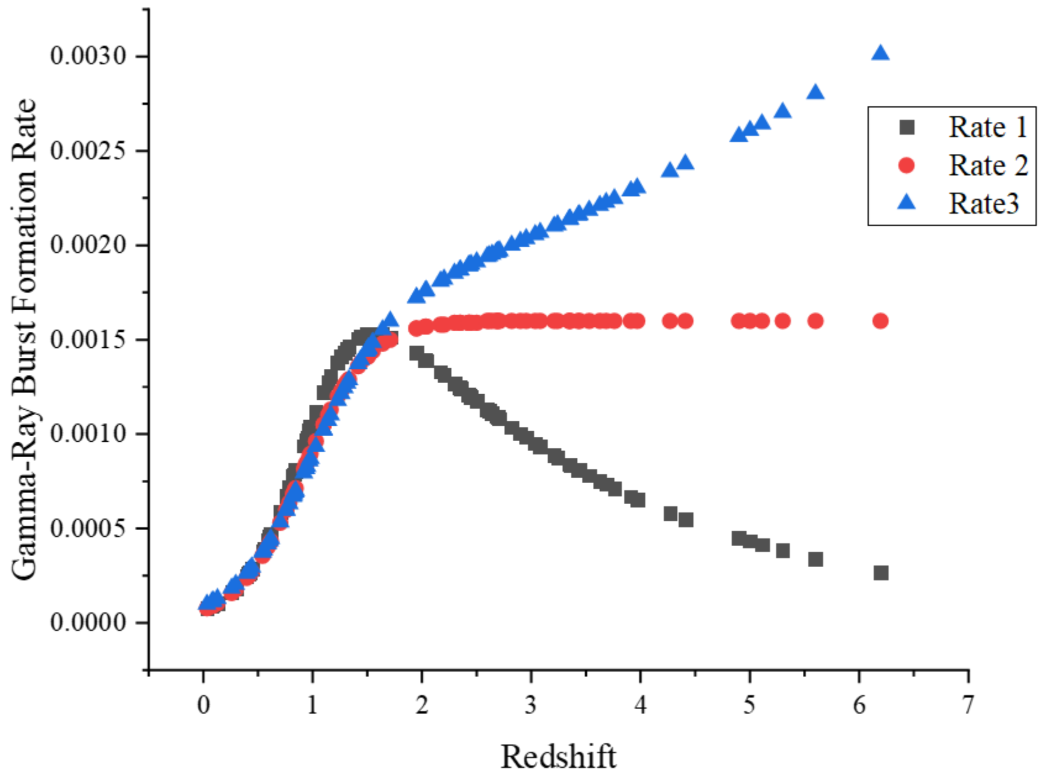

Figure 4.3: Gamma Ray- Burst Formation rate vs. Redshift

The above figure (fig 4.2) tells us that the formation rate of Gamma-Ray Burst is directly related to the star formation rate history of the universe. Because we can see from the graph that if the star formation rate history increase, the formation rate of GRB also increase, if the star formation rate history becomes roughly constant, the formation rate of GRB also becomes constant. If it declines, it also declines. Generally, they have the same pattern of increase and decrease.

In statistics, data from samples are used to understand larger populations. Standard error matters because it helps to estimate how well the sample data represents the whole population. By calculating standard error, we can estimate how representative the sample in the population and make valid conclusions. A high standard error shows that sample means are widely spread around the population mean, a sample may not closely represent the population. A low standard error shows that sample means are closely distributed around the population mean and the sample is representative of the population. The standard error can be decrease by increasing sample size and using a large, random sample is the best way to minimize sampling bias. From the above figure (fig 4.3) the standard error of the gamma-ray burst formation rate is 6.14E-05 and it tells that the sample is well spread around the mean (mean = 1.12E-05) and the sample is representative of the population as it is closely related to the mean of the population.

Next, we are going to evaluate the comoving volume of gamma ray burst per unit redshift and it can be calculated as follows:

$$\frac{dV}{dz} = \frac{4\pi c {D_L}^2}{H(z)} \frac{1}{(1+z)^2}$$

$$D_L = \mathrm{c}(1+\mathrm{z})\int_0^z \frac{1}{H(Z')} \mathrm{d}z'$$

$$\mathrm{H(z)}=H_0[(1z')^3\Omega_m + \Omega_\Lambda + (1 - \Omega_m - \Omega_\Lambda)(1 + z')^2]^{1/2}$$

$$D_L = \mathrm{c}(1+\mathrm{z})\int_i^z \frac{1}{H_0[(1+z')^3\Omega_m+\Omega_\Lambda+(1-\Omega_m-\Omega_\Lambda)(1+z')^2]^{1/2}} \mathrm{d}z'$$

Table 4.1: Calculated values for different quantities of GRB Related Data

GRB	z	H(z)	1/H(z)	Log D_L	dV/dz	R_{SF}	dN/dz
050904	6.3	4818.1	0.00021	4.4484	8.36E-11	0.15	2.19E-14
080913	6.7	4818.1	0.00021	4.69139	3.30E-08	0.15	8.65E-12
090423	8.2	8200.72	0.00012	4.91312	1.38E-08	0.15	3.62E-12
130606A	5.9	3473.84	0.00029	5.08322	5.62E-08	0.15	1.47E-11
140515A	6.3	4109.18	0.00024	5.28065	4.27E-08	0.15	1.12E-11
090429B	9.4	11835.6	8.40E-05	5.57528	7.56E-09	0.15	1.98E-12
120521C	6	3626	0.00028	5.62388	5.24E-08	0.15	1.37E-11
120923A	8.5	9026.94	0.00011	5.79397	1.18E-08	0.15	3.09E-12
050318	1.44	177.031	0.00565	5.86991	5.09E-06	0.121048	1.33E-09
050401	2.9	647.35	0.00154	6.1372	8.04E-07	0.149635	2.11E-10
050416A	0.65	71.6673	0.01395	6.28603	1.17E-05	0.038883	3.06E-09
050525A	0.61	68.3195	0.01464	6.38323	1.18E-05	0.035375	3.10E-09
050802	1.71	233.476	0.00428	6.55636	3.54E-06	0.13606	9.29E-10
050922C	2.2	368.564	0.00271	6.67785	1.86E-06	0.146772	4.89E-10
060206	4.05	1376.77	0.00073	6.82365	2.48E-07	0.14999	6.51E-11
060210	3.91	1267.39	0.00079	6.92388	2.83E-07	0.149985	7.42E-11
060306	3.5	981.313	0.00102	8.36969	4.23E-07	0.149944	1.11E-10
060614	0.13	39.6504	0.02522	8.39399	3.03E-06	0.009599	7.95E-10
060814	1.92	285.919	0.0035	8.49118	2.68E-06	0.142452	7.03E-10
060904A	1.88	275.323	0.00363	8.64002	2.82E-06	0.141499	7.41E-10
060904A	0.94	101.165	0.00988	8.81011	9.41E-06	0.069779	2.47E-09
060904A	5.47	2868.32	0.00035	9.08044	7.66E-08	0.15	2.01E-11

From the above table (table 4.1), H(z) in units of km/sec/Mparsec, D_L in Mparsec, dV/dz in $(\mathrm{Mpc})^3$ and R_{SN} in $M_\odot\,\mathrm{yr}^{-1}\mathrm{Mpc}^{-3}$.

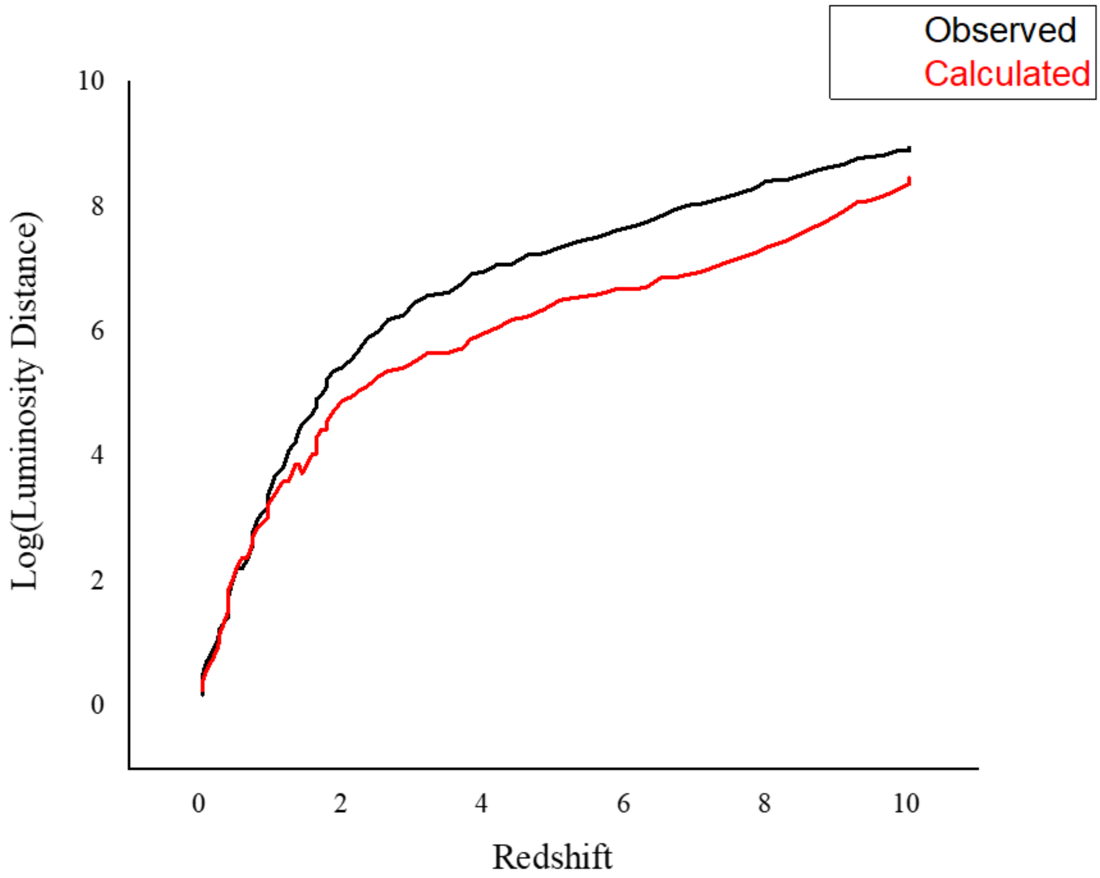

Figure 4.4: The luminosity distance vs. redshift of long gamma ray burst

The observed luminosity distance of fig 4.4 is based on data taken from table 3.4 and the calculated is based on table 4.1. The observe peak flux and fluence of GRB can be calculated as from the given values of redshift, isotropic peak energy and time (T_{90}).

$$S_E^{P,obs} = \int EN\left(E, \alpha, \beta, E_{peak}^{obs}, A^*\right) dE$$

$$\mathrm{S(E)} = \mathrm{A}(E/100Kev)^{\alpha}\exp(-\mathrm{E}/E_{Peak}) \text{ for E } < (\alpha - \beta)\, E_{Peak}$$

Then $$F_E^{P,obs} = \frac{S_E^{P,obs}}{T(1+Z)}$$

The photon number spectrum (S(E)) is fitted with a normalization constant of “A” =0.0125and index of α = -1.25. We took only the α index for the calculation of photon number spectrum because of the band energy of the detector is less than the lower index minus higher index multiplied by the isotropic peak energy of the detector of GRB.

Table 4.2: The calculated peak fluence and flux of GRB from swift satellite

GRB	T_{90} in second	Redshift (z)	$E_{iso}(erg/s)$	Fluence (ergs/cm^2)	Flux (ergs/cm^2)
050126	49.81	1.29	3.60E+51	1.00E-07	8.80E-10
050223	173.36	0.588	5.70E+50	5.11E-06	1.86E-08
050315	3.75	1.949	3.00E+52	1.05E-05	9.46E-07
050318	603.5	1.44	5.80E+51	6.98E-06	4.74E-09
050319	2.30	3.24	3.00E+52	4.70E-06	8.53E-07
050401	180.80	2.9	1.60E+53	3.71E-06	5.26E-09
050505	22.51	4.27	8.80E+52	9.35E-06	7.88E-08
050525A	50.20	0.606	1.50E+52	6.79E-06	8.43E-08
050603	60.0	2.821	1.10E+53	6.13E-06	2.67E-08
050724	69.0	0.258	1.60E+50	9.19E-06	1.06E-07
050730	13.62	3.969	7.50E+52	4.63E-06	6.84E-08
050802	3.06	1.71	1.50E+52	9.75E-06	1.18E-06
050803	135.06	0.422	9.60E+50	3.86E-06	2.01E-08
050814	158.8	5.3	9.90E+52	2.85E-06	2.85E-09
050820A	12.80	2.613	5.40E+52	8.29E-06	1.79E-07
050824	8.21	0.83	4.80E+50	8.09E-06	5.39E-07
050826	12.82	0.297	8.80E+49	4.94E-06	2.97E-07
050904	6.60	6.195	3.00E+53	4.87E-06	1.02E-07
050908	2.16	3.346	1.20E+52	6.66E-06	9.57E-06
051016B	44.5	0.396	3.90E+51	8.76E-06	1.41E-07
051109A	8.66	2.346	2.90E+51	8.57E-06	2.96E-07
051109B	5.0	0.08	3.70E+48	9.19E-06	1.70E-06
051111	24.38	1.549	2.50E+52	6.55E-06	1.05E-07
060108	458	2.03	3.70E+51	3.65E-06	2.63E-09
060115	185.7	3.53	4.50E+52	5.38E-06	6.40E-09
060123	238	1.099	9.50E+50	3.47E-06	6.95E-09
060124	189.4	2.298	5.80E+51	8.98E-06	1.44E-08

5 Conclusion and Recommendation

Our findings imply that Hopkins (2004) was correct in his assertion that the SFR rapidly increases with redshift and that the rate of GRB formation does the same. The star formation rate of GRBs, combined with the comoving rate and the beaming effect of the bursts are then used to predict the redshift distribution for GRBs given a SFR model. Based on the correlation the initial mass function (IMF) of stars and Type II supernova comoving rate. Our results are in a good agreement with those reported recently by Porciani and Madau (Porciani and Madau 2001) about star formation rate. They concerned about the star formation rate of long GRBs. In this work we assume that the GRB formation rate trace the cosmic star formation rates. In previous calculation Bromm & Loeb (2002) (Bromm and Loeb 2002) predicted a higher proportion of GRBs at higher redshifts compared to this work. Depending on their sensitivity to detection and the spread of the GRB, different equipment may find GRBs up to different redshifts (Norris 2002; Schaefer, Deng, and Band 2001; Schmidt 1999). As can be seen from the fig (fig.4.4), the observed and computed luminosity distances were roughly proportionate. The luminosity distance of a gamma ray burst is proportional to that of the gamma ray burst's redshift. The assumption that the SFR is a good proxy for the GRB rate can also be tested further in the near future as the uncertainties due to dust correction in determining SFRs are better understood and the host galaxies of GRBs are studied in more detail.

Research Fund Acknowledgment

This research project is funded by Adama Science and Technology University under the grant number ASTU/SM-R/545/22, Adama, Ethiopia.

References

Abbott, R., Abbott, T. D., Abraham, S., Acernese, F., Ackley, K., Adams, C., ... & Bruno, G. (2021). Search for gravitational waves associated with gamma-ray bursts detected by Fermi and Swift during the LIGO–Virgo run O3a. *The Astrophysical Journal*, **915**(2), 86.

Ackermann, M., Ajello, M., Asano, K., Axelsson, M., Baldini, L., Ballet, J., ... & Siskind, E. J. (2013). The first Fermi-LAT gamma-ray burst catalog. *The Astrophysical Journal Supplement Series*, **209**(1), 11.

Al, Abbott E T. 2008. The Astrophysical Journal , 683: L45–L49, 2008 August 10, 2008.(1): 45–49.

Band, D. L. (2003). Comparison of the gamma-ray burst sensitivity of different detectors. *The Astrophysical Journal*, **588**(2), 945

Barthelmy, S. D., Cline, T. L., Butterworth, P., Kippen, R. M., Briggs, M. S., Connaughton, V., & Pendleton, G. N. (2000, September). GRB Coordinates Network (GCN): A Status Report. In *AIP Conference Proceedings*, **526**(1),731-735). American Institute of Physics.

Bloom, J. S., Frail, D. A., & Kulkarni, S. R. (2003). Gamma-ray burst energetics and the gamma-ray burst Hubble diagram: promises and limitations. *The Astrophysical Journal*, **594**(2), 674.

Bromm, Volker, and Abraham Loeb. 2002. The Expected Redshift Distribution of Gamma-Ray Bursts. *The Astrophysical Journal* **575**(1): 111–16.

Clausen-Brown, E., Savolainen, T., Pushkarev, A. B., Kovalev, Y. Y., & Zensus, J. A. (2013). Causal connection in parsec-scale relativistic jets: results from the MOJAVE VLBI survey. *Astronomy & Astrophysics*, **558**, A144.

Connaughton, V., Briggs, M. S., Goldstein, A., Meegan, C. A., Paciesas, W. S., Preece, R. D., ... & Zhang, B. B. (2015). Localization of gamma-ray bursts using the fermi gamma-ray burst monitor. *The Astrophysical Journal Supplement Series*, **216**(2), 32.

Dermer, C. D. (2002). Gamma ray bursts and cosmic ray origin. preprint astro-ph/0202254.

Dingus, B L, Y Kaneko, R D Preece, and M S Briggs. 2009. broadband , time-dependent , spectroscopy of the brightest bursts observed by batse lad and egret tasc: 2155–69.

Du, Tan-tan et al. 2022. A Study of the Spectral Properties of Two Gamma-Ray Bursts with the Main Bursts and Postbursts.*The Astrophysical Journal* **940**(1): 48.

Fan, Y. Z., & Piran, T. (2008). High-energy γ-ray emission from gamma-ray bursts—before GLAST. *Frontiers of Physics in China*, **3**(3), 306-330.

Fan, Yizhong, and Tsvi Piran. 2006. Gamma-Ray Burst Efficiency and Possible Physical Processes Shaping the Early Afterglow.*Monthly Notices of the Royal Astronomical Society* **369**(1): 197–206.

Frail, D. A., Kulkarni, S. R., Sari, R., Djorgovski, S. G., Bloom, J. S., Galama, T. J., ... & Chaffee, F. (2001). Beaming in gamma-ray bursts: evidence for a standard energy reservoir. *The Astrophysical Journal*, **562**(1), L55.

Frontera, F., Amati, L., Costa, E., Muller, J. M., Pian, E., Piro, L., ... & Sari, R. (2000). Prompt and delayed emission properties of gamma-ray bursts observed with BeppoSAX. *The Astrophysical Journal Supplement Series*, **127**(1), 59.

Gehrels, N., Barthelmy, S. D., Burrows, D. N., Cannizzo, J. K., Chincarini, G., Fenimore, E., ... & Zhang, B. (2008). Correlations of prompt and afterglow emission in Swift long and short gamma-ray bursts. *The Astrophysical Journal*, **689**(2), 1161.

Howell, E. J., & Coward, D. M. (2013). A redshift–observation time relation for gamma-ray bursts: evidence of a distinct subluminous population. *Monthly Notices of the Royal Astronomical Society*, **428**(1), 167-181.

Huang, Y. F., Dai, Z. G., & Lu, T. (2000). On the optical light curves of afterglows from jetted gamma-ray burst ejecta: effects of parameters. *Monthly Notices of the Royal Astronomical Society,* **316**(4), 943-949.

Jones, Tucker, Daniel P Stark, and Richard S Ellis. 2018. Dust in the Wind : Composition and Kinematics of Galaxy Out Fl Ows at the Peak Epoch of Star Formation. *The Astrophysical Journal* **863**(2): 191..

Lan, G. X., Wei, J. J., Zeng, H. D., Li, Y., & Wu, X. F. (2021). Revisiting the luminosity and redshift distributions of long gamma-ray bursts. *Monthly Notices of the Royal Astronomical Society*, **508**(1), 52-68.

Le, T., & Mehta, V. (2017). Revisiting the redshift distribution of Gamma-Ray bursts in the swift era. *The Astrophysical Journal*, **837(**1), 17.

MacFadyen, A. I., & Woosley, S. E. (1999). Collapsars: Gamma-ray bursts and explosions in failed supernovae. *The Astrophysical Journal*, **524**(1), 262.

McGlynn, S., Clark, D. J., Dean, A. J., Hanlon, L., McBreen, S., Willis, D. R., ... & Foley, S. (2007). Polarisation studies of the prompt gamma-ray emission from GRB 041219a using the spectrometer aboard INTEGRAL. *Astronomy & Astrophysics*, **466**(3), 895-904.

Meller, S., Winterberg, F., Gilliet, M., Müller, A., Lauceviciute, I., Rieker, J., ... & Homey, B. (2005). Ultraviolet radiation–induced injury, chemokines, and leukocyte recruitment: an amplification cycle triggering cutaneous lupus erythematosus. Arthritis & Rheumatism, **52**(5), 1504-1516

Metzger, M. R., Djorgovski, S. G., Kulkarni, S. R., Steidel, C. C., Adelberger, K. L., Frail, D. A., ... & Frontera, F. (1997). Spectral constraints on the redshift of the optical counterpart to the γ-ray burst of 8 May 1997. Nature, **387**(6636), 878-880.

Nava, L, G Ghirlanda, G Ghisellini, and C Firmani. 2008. Peak Energy of the Prompt Emission of Long Gamma-Ray Bursts versus Their Fluence and Peak Flux. **652**: 639–52.

Norris, J. P., and J. T. Bonnell. 2006. Short Gamma-Ray Bursts with Extended Emission. *The Astrophysical Journal* **643**(1): 266–75.

Paciesas, W. S., Meegan, C. A., Pendleton, G. N., Briggs, M. S., Kouveliotou, C., Koshut, T. M., ... & Sahi, M. (1999). The fourth BATSE gamma-ray burst catalog (revised). *The Astrophysical Journal Supplement Series*, **122**(2), 465.

Paul, D. (2018). Modelling the luminosity function of long gamma-ray bursts using Swift and Fermi. *Monthly Notices of the Royal Astronomical Society*, **473**(3), 3385-3393

Perlmutter, S. (2000). Supernovae, dark energy, and the accelerating universe: The status of the cosmological parameters. *International Journal of Modern Physics*, **15**, 715-739

Perna, Rosalba, Philip J. Armitage, and Bing Zhang. 2006. "Flares in Long and Short Gamma-Ray Bursts: A Common Origin in a Hyperaccreting Accretion Disk." *The Astrophysical Journal* **636**(1): L29–32.

Piran, T., & Nakar, E. (2010). On The External Shock Synchrotron Model for GRBs' GeV Emission. *arXiv preprint* arXiv:**1003**.5919.

Piran, T. (2000). Gamma-ray bursts–a puzzle being resolved. *Physics Reports*, **333**, 529-553.

Porciani, Cristiano, and Piero Madau. 2001. On the Association of Gamma-Ray Bursts with Massive Stars: Implications for Number Counts and Lensing Statistics. *The Astrophysical Journal* **548**(2): 522–31.

Preece, R. D., Briggs, M. S., Mallozzi, R. S., Pendleton, G. N., Paciesas, W. S., & Band, D. L. (2000). The BATSE gamma-ray burst spectral catalog. I. High time resolution spectroscopy of bright bursts using high energy resolution data. *The Astrophysical Journal Supplement Series***, 126(**1), 19.

Rossi, Elena M, and Robert Mochkovitch. 2006. "The Redshift Distribution of Swift Gamma-Ray Bursts : Evidence for Evolution ´ GRB intrinsic properties. **1042**: 1034–42.

Ryde, F. 2011. "Cosmological Effects on the Observed Flux and Fluence Distributions of Gamma-Ray Bursts : Are the Most Distant Bursts in General the Faintest Ones ? **55**: 1–9.

Dániel, V., Inneman, A., Pína, L., Zadražil, V., Báča, T., Stehlikova, V., ... & Schulz, T. (2017, May). X-ray Lobster Eye all-sky monitor for rocket experiment. In *EUV and X-ray Optics: Synergy between Laboratory and Space* **1023**,102-113). SPIE.

Stanek, K. Z., Dai, X., Prieto, J. L., An, D., Garnavich, P. M., Calkins, M. L., ... & Matheson, T. (2006). Anomalous Optical Gamma-Ray Burst Afterglows Are Common: Two z~ 4 Bursts, GRB 060206 and GRB 060210. *The Astrophysical Journal*, **654**(1), L21.

Steidel, C. C., Adelberger, K. L., Giavalisco, M., Dickinson, M., & Pettini, M. (1999). Lyman-break galaxies at z$\gtrsim$ 4 and the evolution of the ultraviolet luminosity density at high redshift. *The astrophysical journal*, **519**(1), 1.

Stern, B. E., J-L. Atteia, and K. Hurley. 2002. Evidence for a Fast Decline in the Progenitor Population of Gamma-Ray Bursts and the Nature of Their Origin. *The Astrophysical Journal* **578**(1): 304–9.

Della Valle, M. (2007). Supernovae and Gamma Ray Bursts. *Revista Mexicana de Astronomía y Astrofísica*, **30**, 104-109.

Wanderman, D., & Piran, T. (2010). The luminosity function and the rate of Swift's gamma-ray bursts. *Monthly Notices of the Royal Astronomical Society*, **406(**3), 1944-1958.

Wang, Chen, Zhao-yang Peng, and Shun Huang. 2022. A Comprehensive Analysis of Fermi Gamma-Ray Burst Data with Thermal and Non-Thermal Component**. 4**(1): 6–31.

Wang, F. Y. 2013. The High-Redshift Star Formation Rate Derived from Gamma-Ray Bursts: Possible Origin and Cosmic Reionization. *Astronomy and Astrophysics* **556:** 1–7.

Xu, F., Geng, J. J., Wang, X., Li, L., & Huang, Y. F. (2022). Is the birth of PSR J0538+ 2817 accompanied by a gamma-ray burst? *Monthly Notices of the Royal Astronomical Society*, **509**(4), 4916-4922.

Zhang, Bing, and Peter Mészáros. 2004. Gamma-Ray Bursts: Progress, Problems & Prospects. *International Journal of Modern Physics* **19**(15): 2385–2472.